Since January 2020 Elsevier has created a COVID-19 resource centre with free information in English and Mandarin on the novel coronavirus COVID-19. The COVID-19 resource centre is hosted on Elsevier Connect, the company's public news and information website.

Journal of Structural Biology 170 (2010) 172–179

Contents lists available at ScienceDirect

Journal of Structural Biology

journal homepage: www.elsevier.com/locate/yjsbi

Dynamics and orientation of a cationic antimicrobial peptide in two membrane-mimetic systems

Simone Kosol, Klaus Zangger *

Institute of Chemistry/Organic and Bioorganic Chemistry, University of Graz, Heinrichstrasse 28, A-8010 Graz, Austria

ARTICLE INFO

Article history:
Received 29 October 2009
Received in revised form 21 December 2009
Accepted 28 December 2009
Available online 4 January 2010

Keywords:
Peptides
NMR spectroscopy
Membrane-binding
Antimicrobial
Paramagnetic relaxation

ABSTRACT

In order to investigate the functional and structural properties of cationic α-helical peptides in two different membranes, we studied the 20-residue peptide maximin H6 in two membrane-mimetic systems by NMR spectroscopy using partially ^{15}N-labeled peptide and paramagnetic relaxation enhancements. Maximin H6, which is found in skin secretions of frogs of the *Bombinae* family, attacks gram-negative bacteria and acts haemolytically. While the peptide spontaneously folds into similar structures in both neutral dodecylphosphocholine (DPC) and negatively charged sodium dodecyl sulphate (SDS) micelles, its structure is more flexible in SDS as shown by ^{15}N relaxation measurements. In addition, it is bound closer to the surface of the micelle and rotated by ~70° around its helix axis in the negatively charged membrane surrogate compared to the structure in DPC. This might form the basis for peptide–peptide interactions through a GxxxG motif, which could finally lead to membrane disruption and, thus, preferential attack of negatively charged microbial cell walls.

1. Introduction

Cationic α-helical antimicrobial peptides occur in a wide variety of hosts, and show a strong activity against micro-organisms (Boman, 2000; Hancock and Lehrer, 1998). They are, along with other peptides with various secondary structures, part of the innate immune system that protects the host in an unspecific manner. The host organism is protected by the interaction of these peptides with the cytoplasmic membranes of micro-organisms, and (in some cases) also by binding bacterial endotoxin (lipopolysaccharide) (Hancock and Lehrer, 1998). Ultimately, because of problems with increasing microbial resistances towards currently used antibiotics, antimicrobial peptides might be applied as alternative treatments in fighting bacterial infections. Thus, the possible use of antimicrobial peptides as antibiotics is of great interest to the pharmaceutical industry.

Antimicrobial peptides target microbe membranes, which differ from membranes of multi-cellular animals. The exterior surface of the bacterial membrane is negatively charged, due to a high proportion of lipids with phosphate head groups. In contrast, the outer leaflet of eukaryotic cells has almost no net charge (Matsuzaki, 1999; Zasloff, 2002). According to the commonly accepted Shai–Matsuzaki–Huang model, the peptides bind to the membrane surface when targeting cell membranes and, after reaching a critical concentration, penetrate the membrane and reach the interior (Brogden, 2005; Jenssen et al., 2006; Shai, 1999; Yang et al., 2000; Zasloff, 2002). Typically, cationic antimicrobial peptides have less than 50 amino acids, an amphipathic character, and are positively charged due to residues such as arginine or lysine. Both the amphipacity and the cationic charge seem to be the crucial properties for the membrane activity and, therefore, the antimicrobial effect of the peptides. Many studies have addressed the killing mechanism of cationic antimicrobial peptides; however, details of the process remain unclear. When a microorganism is attacked by a peptide, the membrane of the target cell is disrupted by pore formation, which leads to collapse of the transmembrane electrochemical gradient and, finally, to cell death (Shai, 1999; Zasloff, 2002). Further action of peptides on intracellular anionic targets during the killing process has been hypothesized (Friedrich et al., 2000) but is yet to be demonstrated.

A particularly rich source of antimicrobial peptides is amphibian skin, where these peptides serve as a first defence mechanism against bacterial infection in this moist environment (Simmaco et al., 2009). Peptidic skin secretions of frogs of the *Bombinae* family were among the first to be successfully characterized (Kiss and Michl, 1962). The sequence of the peptide maximin H6 (ILGPVIG TIGNVLGGLL KNL-NH_2) was inferred from its cDNA sequence originally isolated from the skin of the toad *Bombina maxima* (Chinese red-belly toad), where maximin H6 is apparently expressed as part of a precursor protein, together with maximin 7 (Lee et al., 2005). *B. maxima* has been found to produce a large variety of antimicrobial peptides (Lai et al., 2002b; Lee et al., 2005). Due to its amidated

* Corresponding author. Fax: +43 316 380 9840.
E-mail addresses: simonekosol@yahoo.de (S. Kosol), klaus.zangger@uni-graz.at (K. Zangger).

1047-8477/$ - see front matter © 2009 Elsevier Inc. All rights reserved.
doi:10.1016/j.jsb.2009.12.026

C-terminus, the peptide has an elevated net charge of + 2. The peptides isolated from skin secretions were grouped into two families, maximin and maximin H (Lai et al., 2002b). They are homologous to bombinin and bombinin H, respectively, (isolated from the *Bombina* species *B. orientalis* and *B. variegata* (Gibson et al., 1991; Mangoni et al., 2000; Simmaco et al., 1991)) to which they show structural and high sequential similarities (Lai et al., 2002b). Here, maximin H6 was chosen as an example of cationic α-helical antimicrobial peptides, as it shows all the typical characteristics of this peptide group; i.e. charge, chain length, amino acid composition and secondary structure. Another important reason for choosing maximin H6 for the present study is its amino acid composition, which is rich in glycine, valine and leucine. These amino acids are relatively affordable in ^{15}N-labeled form, and such isotopically labelled amino acids are necessary for studying the dynamic behaviour of the peptide. Maximin H6 possesses antibacterial and haemolytic activity, as reported for other maximin H peptides (Lai et al., 2002b), and thus can interact with negatively charged and zwitterionic membranes.

Here we describe the comparative analysis of the structure, dynamics and orientation of maximin H6 in two different membrane-mimetics. Sodium dodecyl sulphate (SDS) was used to mimic an anionic membrane environment, while dodecylphosphocholine (DPC) acted as an uncharged membrane surrogate. The peptide adopts similar α-helical conformations in its interactions with both detergents, but the structure is more flexible in SDS micelles, as shown by ^{15}N-relaxation measurements. Maximin H6 is bound closer to the micelle surface in SDS compared to DPC, as determined by paramagnetic relaxation enhancements. The helix shows a rotation of ~70° around its axis between these two membrane mimetics, orienting the consecutive GxxxG motifs found along the backbone further towards the hydrophobic interior. Such an orientation might promote peptide oligomerization in the anionic environment and, thus, could explain the preference of its membrane-lyzing function towards negatively charged membranes.

2. Materials and methods

2.1. Materials

Maximin H6 (ILGPVIG TIGNVLGGLL KNL-NH_2) and partially ^{15}N-labelled maximin H6 (I**LG**P**V**I**G** TI**G**N**VLGGLL** KN**L**-NH_2; ^{15}N-labelled amino acids are indicated by bold letters) were synthesized by Peptide Specialty Laboratories (Heidelberg, Germany), according to the primary structure of maximin H6, as deduced from its cDNA sequence published by Lee et al. (Lee et al., 2005). The selection of amino acids used for ^{15}N labelling was based on affordability. Bacterial strains were purchased at the German Collection of Microorganisms and Cell Cultures (DMSZ).

2.2. Haemolytic activity

Healthy human erythrocytes were used to determine the haemolytic activity of the peptide. Human blood was donated by S.K. (28 year old healthy female) and taken by a physician. The blood was centrifuged and washed four times with 0.9% NaCl solution to remove the plasma. Maximin H6 dissolved in PBS + 1% DMSO (pH 7.4) was added to the erythrocyte suspension (1×10^8 cells/ml in 0.9% NaCl). The suspension was incubated for 2 h at 37 °C and then centrifuged. To determine the extent of haemolysis, the optical density of the supernatant was measured at 451 nm. Hypotonically lyzed erythrocytes were used as a standard for 100% haemolysis. The experiment was repeated three times including positive and negative controls.

2.3. Antimicrobial activity

Antibiotic activity was tested with an inhibition zone assay on agar plates, according to Hultmark et al. (Hultmark et al., 1982). The peptide was serially diluted in H_2O + 1% DMSO. Inhibition zones were measured from wells filled with 5 μl of peptide solutions and in parallel from sterile paper discs (Sigma–Aldrich) loaded with 20 μl peptide solution. Every experiment was repeated three times and disc diameters were accounted for in the data analysis. Bacterial and fungal strains used in this assay were the gram-negative *Escherichia coli* (BL 21), the gram-positive strains *Bacillus subtilis* (DSM1089) and *Enterococcus caccae* (DSM 19114), the fungal strains *Candida parapsilosis* (NBCC 0707, DSM 70125) and *Saccharomyces cerevisiae* (BCY 1020). Bacteria and fungi were grown to an OD_{600} of 0.7 in Luria–Bertani broth (LB) and universal medium for yeasts (YM), respectively. In mid-logarithmic phase, bacteria were diluted in LB medium and approximately 2×10^5 colony forming units (CFU) plated on Petri dishes with LB + 1.5% agar (Sigma–Aldrich), while fungi were diluted in YM and plated on Petri dishes with YM + 1.5% agar. After overnight incubation at 37 °C, the inhibition zone diameters were recorded, and the lethal concentration (LC) was calculated as described by Hultmark et al. (Hultmark et al., 1982). In this assay, LC refers to the lowest peptide concentration that inhibits bacterial growth.

2.4. NMR spectroscopy

For NMR spectra, unlabeled or partially ^{15}N-labelled maximin H6 (1.5 mg) was dissolved in potassium phosphate buffer (50 mM, pH 5.0) containing 200 mM perdeuterated sodium dodecyl sulphate (SDS-d_{25}) or 100 mM perdeuterated dodecylphosphocholine (DPC-d_{38}). Spectra of the peptide were acquired in 90% aqueous buffer/10% ^2H_2O solvent at 300 K on a Bruker AVANCE 500 MHz (5 mm TXI triple-resonance probe with z-axis gradients) and Varian Unity INOVA 600 MHz (5 mm HCN triple-resonance probe with z-axis gradient) NMR spectrometers. The data were processed and analysed manually using NMR-Pipe (Delaglio et al., 1995) and NMRView (Johnson and Blevins, 1994). ^{15}N longitudinal (T_1), ^{15}N transverse (T_2) and {^{1}H}–^{15}N heteronuclear NOE relaxation data (Palmer, 2004) were obtained using relaxation-edited HSQC spectra, and fitted using the NMRView rate analysis tool (Johnson and Blevins, 1994). Relaxation delays from 10 to 5000 ms and 10 to 410 ms were applied for T_1 and T_2 measurements, respectively. The {^{1}H}–^{15}N heteronuclear NOEs were measured from ^{1}H-saturated and unsaturated spectra (3 s saturation time). NMR self-diffusion coefficients and peptide–micelle radii were determined using a stimulated spin-echo experiment, as previously described (Göbl et al., submitted for publication).

2.5. Structure calculation

NMR solution structure calculations were carried out with CNS 1.1 (Brünger et al., 1998) employing the full simulated annealing method. The restraints used for the calculations were Hα proton shifts, NOEs, dihedral angles and hydrogen bonds. The Φ/Ψ dihedral-angle restraints were calculated from chemical shifts of backbone N, Cα and C′ using the program TALOS (Cornilescu et al., 1999). For the structure calculations of maximin H6 in DPC and SDS micelles 271 and 244 NOE restraints were used, respectively. Hydrogen bonds were used as distance restraints for the last steps in the structure refinement only.

2.6. Paramagnetic relaxation enhancement

To obtain paramagnetic relaxation enhancements, the samples were titrated with Gd(DTPA-BMA) (60 mM) to final concentrations

Table 1
Antimicrobial activity of maximin H and maximin peptides.

Microorganism	Peptide			
	Maximin H6	Maximin H5 (Lai et al., 2002a)	Maximin H1 (Lai et al., 2002b)	Maximin 1 (Lai et al., 2002b)
Escherichia coli	+	–	+	+
Bacillus subtilis	–	nd	nd	nd
Enterococcus caccae	–	nd	nd	nd
Bacillus pyocyaneus	nd	–	+	+
Saccharomyces cervisiae	–	nd	nd	nd
Candida parapsilosis	–	nd	nd	nd
Candida albicans	nd	–	+	+
% hemolysis at 100 μM	70	no lysis	90	no lysis

nd = not determined.
+: active.
–: no detectable activity.

of 0.5, 1, 1.5, 2, 3, 4 and 5 mM. Proton T_1 relaxation times were obtained from a series of 2D TOCSY spectra, with a saturation recovery sequence at the beginning, as described for CM15 (Respondek et al., 2007). For each series, the delays between the saturation and start of the actual 2D sequence were 100, 300, 500, 700, 1000, 1500, 2000 and 3000 ms. The tilt and azimuth angles were obtained by fitting Hα-protons to a paramagnetic relaxation wave (Respondek et al., 2007) in Microsoft Excel. To obtain the orientation (including immersion depth) in the micelle we used all PREs within the well-structured region (Val5-Asn19) as input for the program Parapos (Zangger et al., 2009). A radius of 22.6 Å was used for the DPC micelles (Göbl et al., submitted for publication), while a radius of 20 Å was, according to Mazer et al. (Mazer et al., 1976), assumed for SDS micelles.

3. Results and discussion

3.1. Bioactivity

To test the antibacterial activity of maximin H6, a gram-negative (*E. coli*) and two gram-positive (*B. subtilis* and *E. caccae*) species were used. Maximin H6 inhibits the growth of *E. coli* at low peptide concentrations (LC 2.8 ± 0.5 μM) (Table 1), which is in accordance with earlier studies of other maximin H peptides (Lai et al., 2002b). Although Lai et al. (Lai et al., 2002b) found that other maximin H peptides have inhibitory effects on gram-positive bacteria this was not true for maximin H6, which shows no detectable activity against *B. subtilis* and *E. caccae* (Table 1). Maximin H6 possesses strong haemolytic activity (70% lysis) when assayed against human erythrocytes. This is consistent with the findings for other maximin H peptides lyzing up to 90% of rabbit red blood cells (Lai et al., 2002b). Most naturally occurring antimicrobial peptides do not affect erythrocytes (Shai, 2002), because of their low affinity for zwitterionic membranes, which are the major component of the outer leaflet of red blood cells (Verkleij et al., 1973). However, some cationic peptides still bind and sometimes lyze erythrocytes –probably due to the negatively charged carbohydrate moieties on the cell surface, which consist mainly of glycoproteins and glycosphingolipids (Shai, 2002). The growth of the tested fungal strains of *C. parapsilosis* and *S. cerevisiae* was not influenced to

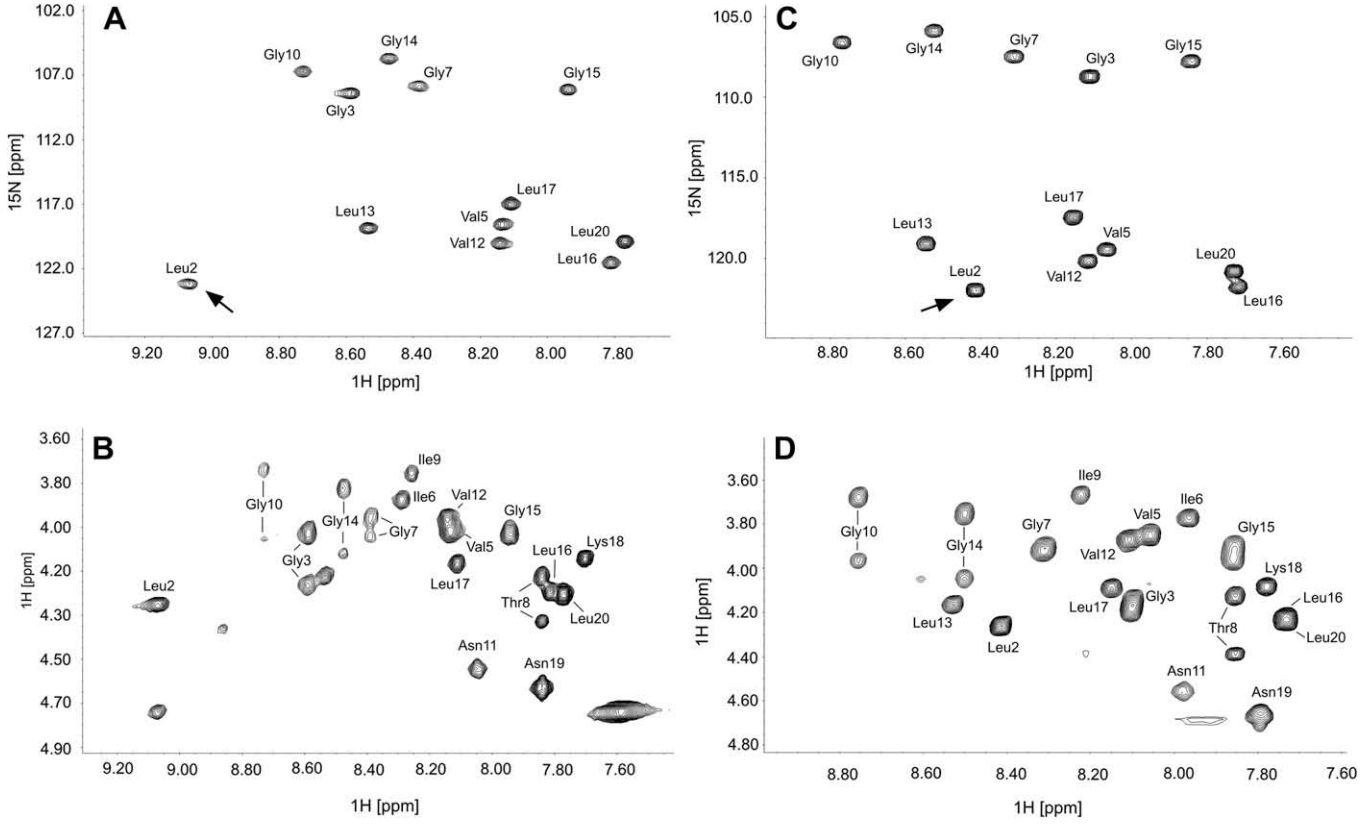

Fig. 1. ^{15}N-^{1}H-HSQC (A) and (C) and fingerprint regions of TOCSY spectra (B) and (D) of maximin H6 in DPC (A) and (B) and SDS (C) and (D) micelles. Unlabeled peptide was used for the TOCSY and partially ^{15}N-labeled peptide for the HSQC spectra. The most significantly shifted amide signal of Leu2 is indicated by arrows.

any detectable level by maximin H6. According to Shai (Shai, 2002), there is a correlation between the hydrophobicity of the peptide and its ability to self-associate and therefore its antifungal action. Although maximin H6 is hydrophobic and has several Gly residues – indicating a possible interaction via a GxxxG motif (Unterreitmeier et al., 2007) – no activity against fungi was found up to peptide concentrations of 1 mM. Thus, of all the organisms tested, maximin H6 only inhibited the growth of gram negative *E. coli*, and lyzed the relatively fragile erythrocytes. Therefore, maximin H6 is clearly not active against a wide variety of microbes, but is rather specific; probably due to its ability to interact and permeate negatively charged and zwitterionic membranes, with a preference towards simpler bacterial membranes. As most multicellular organisms express cocktails of variously structured antibiotic peptides with a range of inhibition abilities, selectivity for specific microbes was also expected among maximin H peptides.

3.2. Structure and dynamics

While X-ray crystallography has so far been unsuccessful in elucidating the structures of small membrane-bound peptides, NMR spectroscopy allows not only the structure, but also dynamics and mode of membrane-binding to be determined (Haney et al., 2009).

Upon dissolving maximin H6 in an aqueous phosphate buffer close to neutral pH, it showed poor chemical-shift dispersion quite typical for random-coil peptides. Addition of SDS-d_{25} or DPC-d_{38} led to large shift changes, up to concentrations of around 120 mM SDS or 70 mM DPC. Thus, to ensure that all of the peptide is bound to micelles, concentrations of 200 mM SDS or 100 mM DPC were used for all subsequent experiments. The proton, carbon and nitrogen signals of maximin H6 were assigned using TOCSY, NOESY, ^{1}H-^{13}C-HSQC on unlabelled peptide as well as ^{1}H-^{15}N-HSQC and NOESY-^{1}H-^{15}N-HSQC spectra on partially ^{15}N-labelled maximin H6. The ^{1}H-^{15}N-HSQC spectra and fingerprint regions of the TOCSY spectra of maximin H6 in SDS and DPC micelle solutions can be seen in Fig. 1. While most resonances have similar chemical shifts in the two systems, indicative of similar three-dimensional structures, the most striking difference is the large difference in the backbone amide protons of Leu2 in the two membrane-mimetics. The corresponding signal is shifted by almost 1 ppm upfield (to lower frequency) in SDS micelles. Backbone amide protons close to the N-terminus are usually found at high frequencies. This is a result of their proximity to the positively charged NH_3^+ group at the N-terminus. The lower electron density of the NH, especially when it forms an H-bond to the NH_3^+ group, leads to enhanced chemical shielding and, thus, to higher frequencies. While this is found in neutral DPC micelles (Fig. 1a and b), the shift to lower frequencies in SDS micelles indicates an increased electron density near the N-terminus. We believe that an ionic interaction between the N-terminal NH_3^+ group with the negatively charged SDS molecules is the reason for this difference in chemical shift. Such an ionic interaction is not possible in the zwitterionic DPC micelles.

Both the sequential NOEs and chemical shift index (CSI) are indicative for mainly α-helical conformations both in DPC and SDS micelles (Fig. 2). The solution structure in DPC was determined using 271 NOEs, together with 12 dihedral-angle restraints, which were obtained using the program TALOS with chemical shifts of Hα, Cα and Cβ nuclei. For the structure calculation in SDS, 244 NOEs and 15 dihedral-angle restraints were used together with chemical shifts of H, Cα and Cβ nuclei. At a later stage in the structure refinement, C'O to NH hydrogen-bond restraints were introduced for residues involved in the α-helix, based on their typical NOE pattern, chemical shifts and TALOS-derived ϕ and ψ angles. A total of 100 structures were calculated; the 20 lowest-energy structures of maximin H6 are shown in Fig. 3 as a least-squares

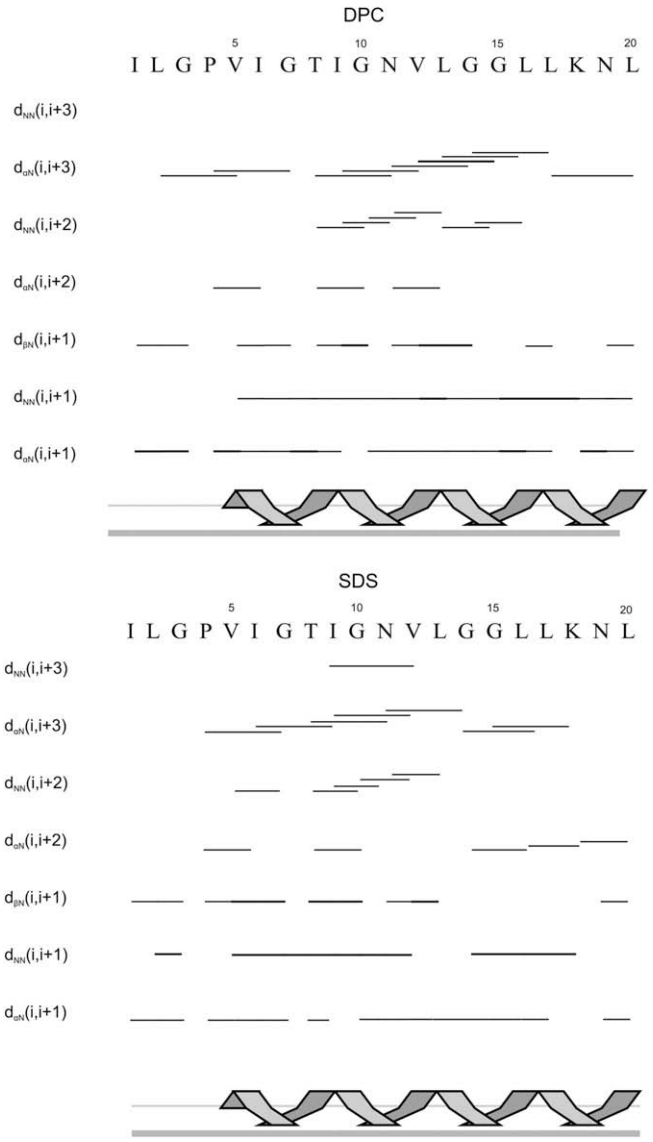

Fig. 2. Sequential NOEs and secondary structure, derived from the consensus chemical shift index CSI (lower part), of maximin H6 in DPC and SDS micelles.

fit bundle, showing only the backbone (Fig. 3a and c), or also the side-chain nuclei (Fig. 3b and d). In both membrane mimics an α-helix is formed: in DPC between residues 5 and 19, with the N-terminal 4 residues (up to Pro4) and the C-terminus being less well-defined. A slight kink can be seen near residue Val12 in DPC micelles. In SDS, the α-helix is formed from residues 5 to 15. In DPC, the rmsd between residues 4 and17 is 0.20 Å and 0.97 Å for the backbone and side-chain atoms, respectively, whereas in SDS micelles the rmsd between residues 4 and 17 is 0.24 Å for the backbone and 0.78 Å for side-chain atoms. A list of structural statistics of maximin H6 in DPC and SDS micelles can be found in Table 2.

In order to investigate the dynamic behaviour of maximin H6 in SDS and DPC micelles, we determined their longitudinal (T_1) and transverse (T_2) relaxation times as well as $\{^{1}H\}^{15}N$-NOEs of partially ^{15}N-labeled maximin H6 (Fig. 4). The peptide shows a quite rigid structure between residues 5 and 18 in both micelle systems (high T_1, low T_2 and high hetero NOEs) with more flexibility at the N- and C-termini. However, even at the termini, the peptide cannot be described as freely flexible, as such a situation would be characterized by negative $\{^{1}H\}^{15}N$-NOEs. The relaxation data also show that maximin H6 is more mobile in SDS. This enhanced flexibility

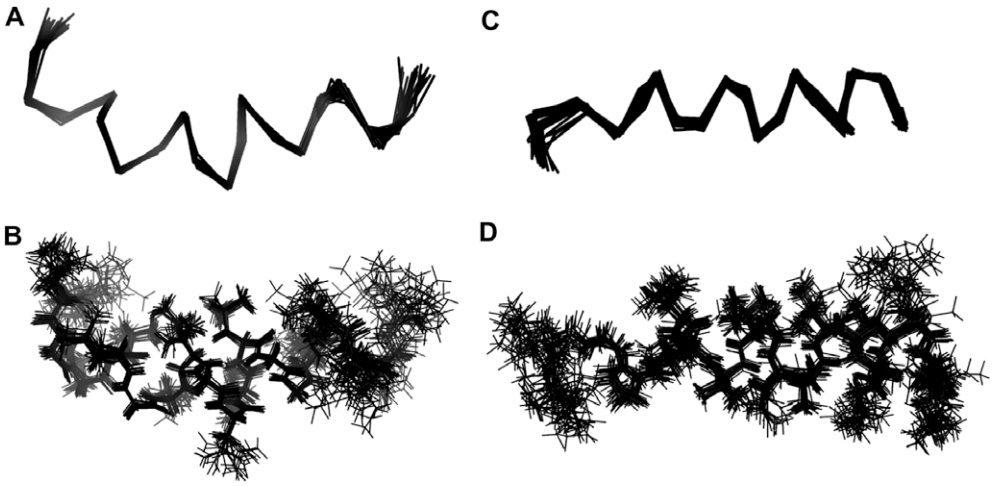

Fig. 3. Least-square superposition of the backbone and side-chain atoms of the 20 lowest-energy structures of maximin H6 in DPC (A, B) and SDS micelles (C, D). The backbone atoms of residues 4–17 were used for the fitting, giving a rmsd of 0.20 and 0.24 in DPC and SDS, respectively.

Table 2
Structural restraints and statistics for the ensemble of 20 lowest-energy structures of maximin H6 in DPC and SDS micelles.

	DPC	SDS
Restraints		
Intraresidue NOEs	155	126
Sequential NOEs (i to i + 1)	66	70
Medium range NOEs (i to i+2,3,4)	50	48
Total NOEs	271	244
Dihedral-angle restraints	12	15
Structural statistics		
Rmsd for backbone atoms (residues 4–17)	0.20	0.24
Rmsd for all atoms (residues 4–17)	0.97	0.78
Rmsd for backbone atoms (residues 1–20)	0.46	0.52
Rmsd for all atoms (residues 1–20)	1.36	1.35
Number of NOE violations > 0.5 Å	0	0
Number of dihedral angle violations > 5°	0	0
Rmsd for covalent bonds (Å)	0.004 ± 0.0002	0.003 ± 0.0001
Rmsd for covalent angles (°)	0.58 ± 0.02	0.53 ± 0.01
Rmsd for improper angles (°)	0.43 ± 0.03	0.28 ± 0.02
Residues in most favored regions of Ramachandran plot (%)	91.7	80.6
Residues in additional allowed regions of Ramachandran plot (%)	8.3	19.4
Residues in generously allowed regions of Ramachandran plot (%)	0.0	0.0
Residues in disallowed regions of Ramachandran plot (%)	0.0	0.0
Energies (kcal/mol)		
Total	117.0 ± 3.6	60.6 ± 2.7
Bond	3.9 ± 0.4	2.2 ± 0.2
Angle	28.4 ± 1.8	23.5 ± 0.9
Improper	3.9 ± 0.6	1.6 ± 0.3
Van der Waals	35.0 ± 2.5	13.8 ± 1.2
NOE	28.9 ± 2.9	13.8 ± 1.1
Dihedral	0.2 ± 0.1	1.1 ± 0.2

in SDS micelles is probably the reason for the α-helix being better defined for a longer stretch in DPC micelles. The rmsd for the backbone between the two mean structures of maximin H6 in DPC and in SDS micelles is 1.14 (for residues 5–17).

The sizes of the peptide–micelle assemblies were determined using NMR self-diffusion measurements. The radii of the micelles as determined on the peptide signals are 22.8 ± 1.5 Å in DPC and 24.2 ± 2.8 Å in SDS micelles. These sizes agree quite well with other peptides of similar length bound to such membrane-mimetics (Göbl et al., submitted for publication) and, thus, do not indicate aggregation of the peptides. However, it should be noted that aggregation is not likely in such detergent micelles due to their small size and surface curvature.

3.3. Orientation in the micelles

To obtain the orientation (tilt and azimuth angles) as well as the immersion depth of maximin H6 in membrane surrogates, we used relaxation enhancements caused by the inert and water-soluble paramagnetic agent Gd(DTPA-BMA) on longitudinal T_1 relaxation times of NMR detectable signals (Respondek et al., 2007; Zangger et al., 2009). Adding this compound to the solvent renders the environment surrounding the micelles paramagnetic, and leads to relaxation enhancements, which depend on the distance to the surface of the biomolecular assembly (Madl et al., 2009; Madl et al., 2006; Pintacuda and Otting, 2002). Depending on the orientation of an α-helical peptide, the PREs oscillate with a periodicity of 3.6 residues (Respondek et al., 2007). The azimuth and rotation angles of helical peptides can be obtained from PREs using paramagnetic relaxation wave fitting (Respondek et al., 2007). The corresponding waves of Hα protons for maximin H6 in DPC and SDS micelles are shown in Fig. 5. Only the well-structured helical region from residues Pro4- Gly15 was used for the fitting procedure. While the tilt angles for the peptide in both micelle systems (7° in DPC and −5° in SDS) show orientations basically parallel to the surface, there are significant deviations in the azimuth (rotation) angles. The azimuth angle ρ (the rotation of the first α-proton of the fitted region) is 80° in DPC and 11° in SDS micelles. Thus, while in zwitterionic DPC micelle residues G7, N11 and G15 point towards the outside, the helix is rotated by ~70° in SDS, so that here residues V5, T8 and V12 are furthest away from the hydrophobic interior. Helical-wheel representations corresponding to the obtained azimuth angles (Fig. 6) indicate the relative orientation of the hydrophobic and hydrophilic regions as well as the pronounced consecutive GxxxG motif close to the hydrophobic–hydrophilic transition. The hydrophobic moment was calculated using the hydrophobicity scales of Wimley and White (Wimley and White, 1996), and is derived from the thermodynamic transfer free energies between water and interface. While the orientation found in DPC micelles is close to what one would expect based on the hydrophobic moment, the orientation in SDS is rotated ~70° counter-clockwise when viewed from the N-terminus. This places the GxxxG motif further towards the hydrophobic environment, and the hydrophobic side of the peptide is moved slightly closer to the outside of the micelle. GxxxG motifs are involved in

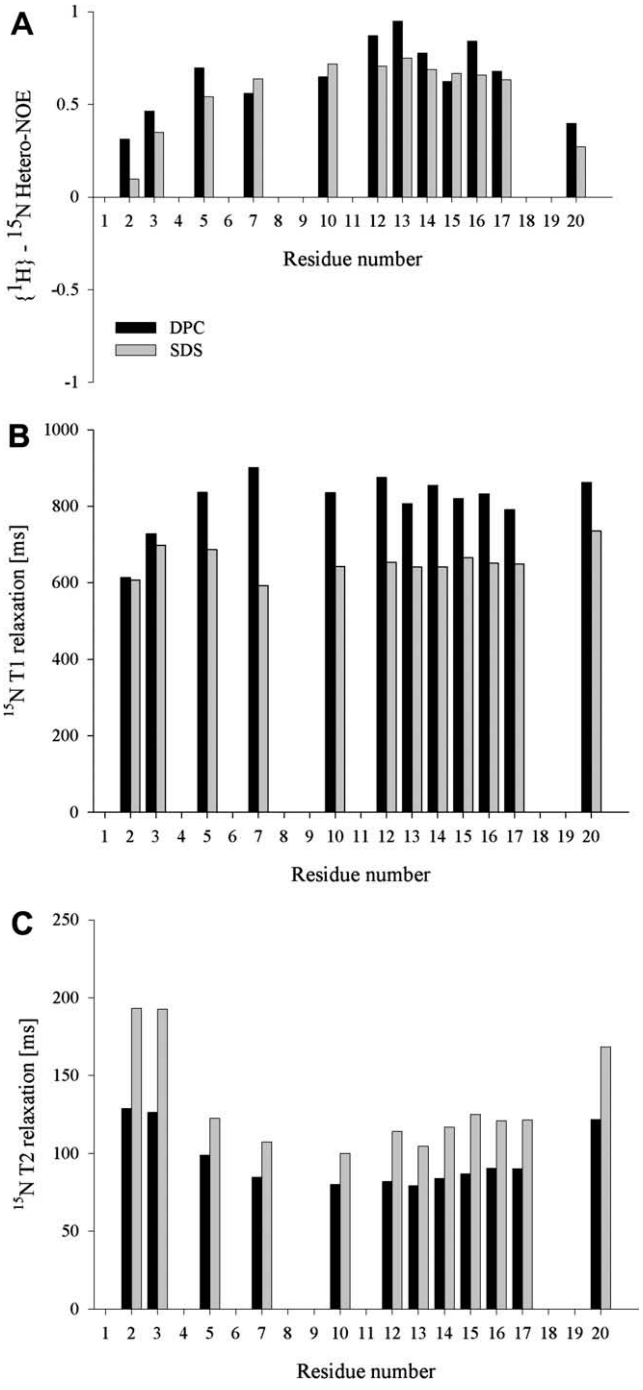

Fig. 4. $\{^1H\}$-^{15}N-NOEs (A), longitudinal (B) and transverse (C) relaxation data for partially N-15 labelled maximin H6 in DPC (black) and SDS (grey) micelles given as a function of residue number.

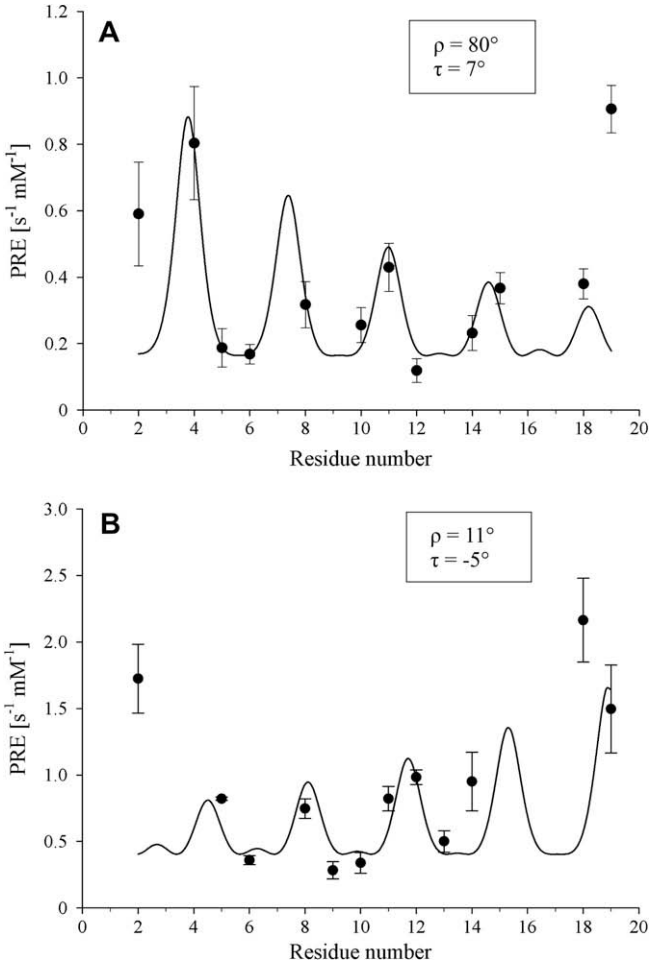

Fig. 5. Paramagnetic relaxation waves for maximin H6 in DPC (A) and SDS (B) micelles. The wave functions were fitted in Microsoft Excel using the α-proton PRE values of residues 4–15.

transmembrane helix dimerization and oligomerization. They have been found, for example, in the influenza hemagglutinin fusion peptide (Chernomordik and Kozlov, 2003; Tamm, 2003), in Alzheimer's peptides (D'Ursi et al., 2004; Sato et al., 2009), in the SARS coronavirus spike protein transmembrane domain (Arbely et al., 2006), and in the antimicrobial peptide bombinin H2 and H4 (Zangger et al., 2008). Negatively charged SDS micelles are membrane mimetics of prokaryotic cells, and the neutral DPC resembles a situation more similar to eukaryotic cell membranes. Therefore, we believe that the rotation around the helix axis in SDS positions the glycine ridge so that it is more likely to form peptide–peptide interactions. Such peptide aggregation events are necessary for the proposed models of antimicrobial peptide action; i.e., the carpet, barrel-stave or the torroidal pore mechanisms (Shai, 1999). Further insight into the exact mode of binding to a micelle, in particular the immersion depth, can be obtained by the least-squares fitting of all (backbone and sidechain) PREs using the program Parapos (Zangger et al., 2009). We used only the well-structured helical regions (Val5-Asn19) for determining the immersion depths as the first 3–4 and last 1 residues show increased flexibility in relaxation measurements. The resulting orientation and location inside their corresponding micelles are shown in Fig. 7. Both peptides bind more or less parallel to the surface, and are inserted just below the polar–nonpolar interface. Maximin H6 is found immersed deeper into DPC micelles, probably due to the larger zwitterionic phosphocholine groups compared to the thinner layer of anionic sulphate groups in SDS. Due to the deeper immersion in DPC micelles there is less space available for the α-helix. This might be the reason for the helix being slightly bent in DPC solution. The positioning of maximin H6 closer to the surface in SDS micelles is also in agreement with its upfield shift of the amide proton of Leu2. The ionic interaction of the positively charged N-terminal NH_3^+-*group* (together with the charge of Lys-18) with the negative charge on the outside of the SDS micelles positions the peptide closer to the surface.

Further useful information that can be obtained from PREs in a paramagnetic environment of peptides bound to micelles pertains

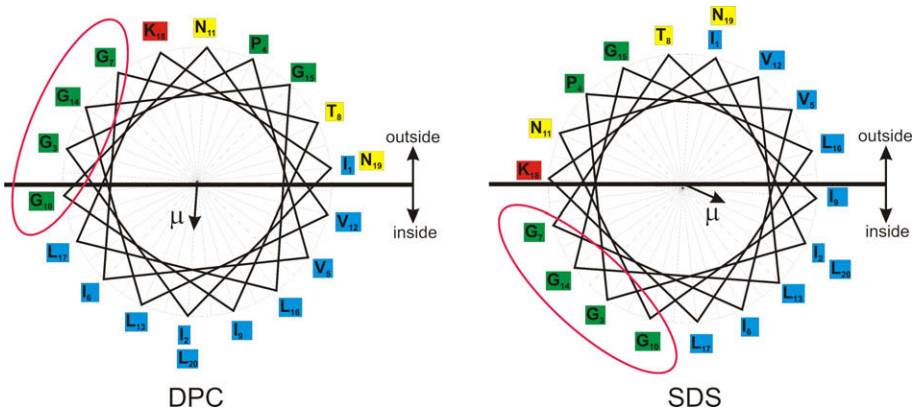

Fig. 6. Helical wheel representation of maximin H6 showing the orientation determined by paramagnetic relaxation waves in DPC and SDS micelles. Hydrophobic, charged, uncharged polar and other residues are coloured blue, red, yellow and green, respectively. The hydrophobic moment is indicated by an arrow and the GxxxG motif is highlighted in a red ellipse.

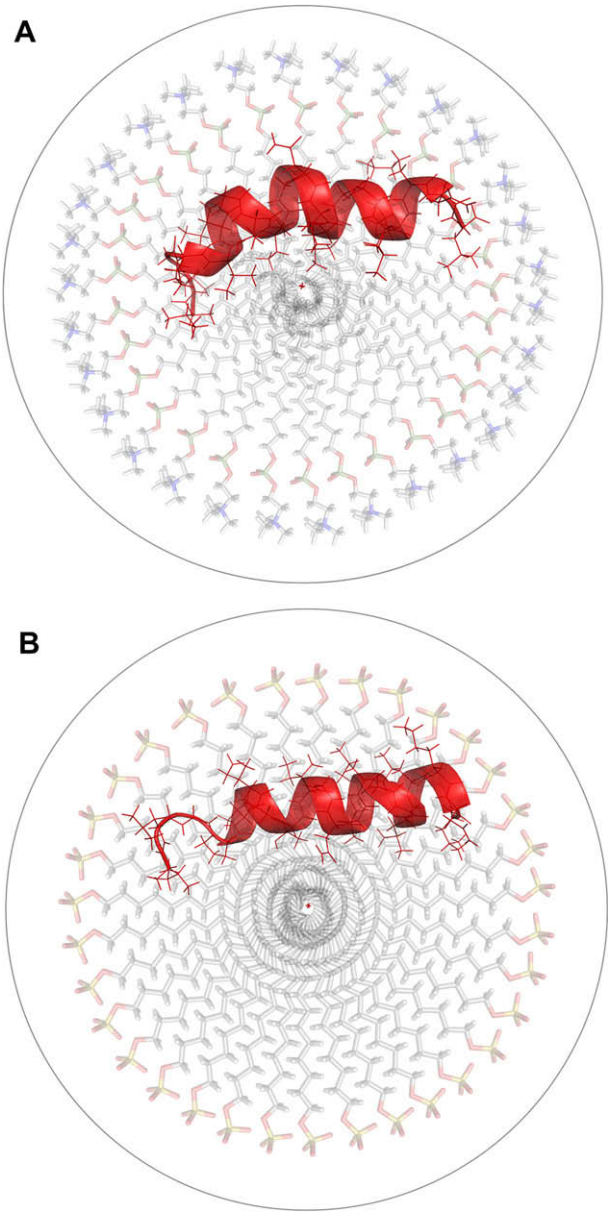

Fig. 7. Immersion of maximin H6 in DPC (A) and SDS (B) micelles as obtained using the program Parapos. The center of each micelle is indicated by a cross. The micelles are drawn to scale and the detergent molecules depicted schematically as stick models. The layer of the closest approaching paramagnetic centers is indicated by a thin grey circle.

to their flexibility. Residues near the termini show unusually large PREs (see Supplementary data). This can be explained by the $1/r^6$ averaging of PREs towards smaller nucleus–paramagnetic center distances "r" (Madl et al., 2009). If a specific nucleus spends only a short time close to a paramagnetic center it shows large PREs. In contrast, NOEs that are averaged to small inter-proton distances result in more compact structures. Therefore, differences between the NOE-derived structure of a micelle-bound peptide and PREs in a paramagnetic environment indicate different flexibility. This is confirmed by comparison with our ^{15}N relaxation data. While the PRE data are represented quite well by the paramagnetic relaxation wave in the α-helical regions, the flexible terminal residues (in particular near the N-terminus) have very high PREs, which cannot be explained by a single NMR conformation. This reduced flexibility in DPC probably results from maximin H6 being immersed deeper into DPC compared to SDS micelles. That might enable the peptide to more readily rotate the GxxxG motif for finding other peptide binding partners in SDS micelles. The dimensions of the peptide–micelle assemblies, as determined by self-diffusion experiments, do not indicate dimerization or formation of larger aggregates. In addition, we did not find any NOEs that do not fit a monomeric structure. Therefore, we have no indication for peptide–peptide interactions in the micelles. However, their behaviour might be different in bacterial or erythrocyte membranes, which exhibit a lower lateral packing density and a more relaxed surface curvature.

In conclusion, by using solution NMR spectroscopy, we have found that the cationic α-helical antimicrobial peptide maximin H6 binds to both negatively charged and zwitterionic membrane-mimetics. The three-dimensional structures formed in the two in membrane-mimetics are similar. However, in the SDS micelles, the peptide is more flexible and bound closer to the surface, and is rotated by around 70° relative to the neutral DPC micelles, thereby orienting a GxxxG further inside the SDS micelle. The location closer to the surface in SDS is likely provided by the interaction of the negatively charged surface with the positive charges of the peptide. Together with a more favourable interaction of the GxxxG motif, this might form the basis for peptide–peptide interactions leading finally to membrane disruption of microbial cell walls by cationic antimicrobial peptides.

Acknowledgements

Financial support by the Austrian Science Foundation (Fonds zur Förderung der wissenschaftlichen Forschung, FWF) under project number 20020 to K.Z. is gratefully acknowledged.

Appendix A. Supplementary data

Supplementary data associated with this article can be found, in the online version, at doi:10.1016/j.jsb.2009.12.026.

References

Arbely, E., Granot, Z., Kass, I., Orly, J., Arkin, I.T., 2006. A trimerizing GxxxG motif is uniquely inserted in the severe acute respiratory syndrome (SARS) coronavirus spike protein transmembrane domain. Biochemistry 45, 11349–11356.

Boman, H.G., 2000. Innate immunity and the normal microflora. Immunol. Rev. 173, 5–16.

Brogden, K.A., 2005. Antimicrobial peptides: pore formers or metabolic inhibitors in bacteria? Nat. Rev. Microbiol. 3, 238–250.

Brünger, A.T., Adams, P.D., Clore, G.M., DeLano, W.L., Gros, P., Grosse-Kunstleve, R.W., Jiang, J.S., Kuszewski, J., Nilges, M., Pannu, N.S., Read, R.J., Rice, L.M., Simonson, T., Warren, G.L., 1998. Crystallography & NMR system: a new software suite for macromolecular structure determination. Acta Crystallogr., D 54, 905–921.

Chernomordik, L.V., Kozlov, M.M., 2003. Protein–lipid interplay in fusion and fission of biological membranes. Annu. Rev. Biochem. 72, 175–207.

Cornilescu, G., Delaglio, F., Bax, A., 1999. Protein backbone angle restraints from searching a database for chemical shift and sequence homology. J. Biomol. NMR 13, 289–302.

D'Ursi, A.M., Armenante, M.R., Guerrini, R., Salvadori, S., Sorrentino, G., Picone, D., 2004. Solution structure of amyloid beta-peptide (25–35) in different media. J. Med. Chem. 47, 4231–4238.

Delaglio, F., Grzesiek, S., Vuister, G.W., Zhu, G., Pfeifer, J., Bax, A., 1995. NMRPipe: a multidimensional spectral processing system based on UNIX pipes. J. Biomol. NMR 6, 277–293.

Friedrich, C.L., Moyles, D., Beveridge, T.J., Hancock, R.E., 2000. Antibacterial action of structurally diverse cationic peptides on gram-positive bacteria. Antimicrob. Agents Chemother. 44, 2086–2092.

Gibson, B.W., Tang, D.Z., Mandrell, R., Kelly, M., Spindel, E.R., 1991. Bombinin-like peptides with antimicrobial activity from skin secretions of the Asian toad, *Bombina orientalis*. J. Biol. Chem. 266, 23103–23111.

Göbl, C., Dulle, M., Hohlweg, W., Grossauer, J., Falsone, S.F., Glatter, O., Zangger, K., submitted for publication. Influence of phosphocholine alkyl chain length on peptide–micelle interactions and micellar size and shape. J. Phys. Chem.

Hancock, R.E., Lehrer, R., 1998. Cationic peptides: a new source of antibiotics. Trends Biotechnol. 16, 82–88.

Haney, E.F., Hunter, H.N., Matsuzaki, K., Vogel, H.J., 2009. Solution NMR studies of amphibian antimicrobial peptides: linking structure to function? Biochim. Biophys. Acta 1788, 1639–1655.

Hultmark, D., Engstrom, A., Bennich, H., Kapur, R., Boman, H.G., 1982. Insect immunity: isolation and structure of cecropin D and four minor antibacterial components from *Cecropia pupae*. Eur. J. Biochem. 127, 207–217.

Jenssen, H., Hamill, P., Hancock, R.E., 2006. Peptide antimicrobial agents. Clin. Microbiol. Rev. 19, 491–511.

Johnson, B.A., Blevins, R.A., 1994. A computer program for the visualization and analysis of NMR data. J. Biomol. NMR 4, 603–614.

Kiss, G., Michl, H., 1962. On the venomous skin secretions of the orange-speckled frog *Bombina variegata*. Toxicon 1, 33–37.

Lai, R., Liu, H., Hui Lee, W., Zhang, Y., 2002a. An anionic antimicrobial peptide from toad *Bombina maxima*. Biochem. Biophys. Res. Commun. 295, 796–799.

Lai, R., Zheng, Y.T., Shen, J.H., Liu, G.J., Liu, H., Lee, W.H., Tang, S.Z., Zhang, Y., 2002b. Antimicrobial peptides from skin secretions of Chinese red belly toad *Bombina maxima*. Peptides 23, 427–435.

Lee, W.H., Li, Y., Lai, R., Li, S., Zhang, Y., Wang, W., 2005. Variety of antimicrobial peptides in the *Bombina maxima* toad and evidence of their rapid diversification. Eur. J. Immunol. 35, 1220–1229.

Madl, T., Bermel, W., Zangger, K., 2009. Use of relaxation enhancements in a paramagnetic environment for the structure determination of proteins using NMR spectroscopy. Angew. Chem., Int. Ed. Engl. 48, 8259–8262.

Madl, T., Van Melderen, L., Mine, N., Respondek, M., Oberer, M., Keller, W., Khatai, L., Zangger, K., 2006. Structural basis for nucleic acid and toxin recognition of the bacterial antitoxin CcdA. J. Mol. Biol. 364, 170–185.

Mangoni, M.L., Grovale, N., Giorgi, A., Mignogna, G., Simmaco, M., Barra, D., 2000. Structure-function relationships in bombinins H, antimicrobial peptides from Bombina skin secretions. Peptides 21, 1673–1679.

Matsuzaki, K., 1999. Why and how are peptide–lipid interactions utilized for self-defense? Magainins and tachyplesins as archetypes. Biochim. Biophys. Acta 1462, 1–10.

Mazer, N.A., Benedek, G.B., Carey, M.C., 1976. An investigation of the micelllar phase of sodium dodecyl sulfate in aqueous sodium chloride solutions using quasielastic light scattering spectroscopy. J. Phys. Chem. 80, 1075–1085.

Palmer 3rd, A.G., 2004. NMR characterization of the dynamics of biomacromolecules. Chem. Rev. 104, 3623–3640.

Pintacuda, G., Otting, G., 2002. Identification of protein surfaces by NMR measurements with a paramagnetic Gd(III) chelate. J. Am. Chem. Soc. 124, 372–373.

Respondek, M., Madl, T., Göbl, C., Golser, R., Zangger, K., 2007. Mapping the orientation of helices in micelle-bound peptides by paramagnetic relaxation waves. J. Am. Chem. Soc. 129, 5228–5234.

Sato, T., Tang, T.C., Reubins, G., Fei, J.Z., Fujimoto, T., Kienlen-Campard, P., Constantinescu, S.N., Octave, J.N., Aimoto, S., Smith, S.O., 2009. A helix-to-coil transition at the epsilon-cut site in the transmembrane dimer of the amyloid precursor protein is required for proteolysis. Proc. Natl. Acad. Sci. USA 106, 1421–1426.

Shai, Y., 1999. Mechanism of the binding, insertion and destabilization of phospholipid bilayer membranes by alpha-helical antimicrobial and cell non-selective membrane-lytic peptides. Biochim. Biophys. Acta 1462, 55–70.

Shai, Y., 2002. Mode of action of membrane active antimicrobial peptides. Biopolymers 66, 236–248.

Simmaco, M., Kreil, G., Barra, D., 2009. Bombinins, antimicrobial peptides from Bombina species. Biochim. Biophys. Acta 1788, 1551–1555.

Simmaco, M., Barra, D., Chiarini, F., Noviello, L., Melchiorri, P., Kreil, G., Richter, K., 1991. A family of bombinin-related peptides from the skin of *Bombina variegata*. Eur. J. Biochem. 199, 217–222.

Tamm, L.K., 2003. Hypothesis: spring-loaded boomerang mechanism of influenza hemagglutinin-mediated membrane fusion. Biochim. Biophys. Acta 1614, 14–23.

Unterreitmeier, S., Fuchs, A., Schaffler, T., Heym, R.G., Frishman, D., Langosch, D., 2007. Phenylalanine promotes interaction of transmembrane domains via GxxxG motifs. J. Mol. Biol. 374, 705–718.

Verkleij, A.J., Zwaal, R.F., Roelofsen, B., Comfurius, P., Kastelijn, D., van Deenen, L.L., 1973. The asymmetric distribution of phospholipids in the human red cell membrane. A combined study using phospholipases and freeze-etch electron microscopy. Biochim. Biophys. Acta 323, 178–193.

Wimley, W.C., White, S.H., 1996. Experimentally determined hydrophobicity scale for proteins at membrane interfaces. Nat. Struct. Biol. 3, 842–848.

Yang, L., Weiss, T.M., Lehrer, R.I., Huang, H.W., 2000. Crystallization of antimicrobial pores in membranes: magainin and protegrin. Biophys. J. 79, 2002–2009.

Zangger, K., Gossler, R., Khatai, L., Lohner, K., Jilek, A., 2008. Structures of the glycine-rich diastereomeric peptides bombinin H2 and H4. Toxicon 52, 246–254.

Zangger, K., Respondek, M., Gobl, C., Hohlweg, W., Rasmussen, K., Grampp, G., Madl, T., 2009. Positioning of micelle-bound peptides by paramagnetic relaxation enhancements. J. Phys. Chem. B 113, 4400–4406.

Zasloff, M., 2002. Antimicrobial peptides of multicellular organisms. Nature (London, United Kingdom) 415, 389–395.